FEASIBILITY OF ECCENTRIC FIBRE PRESTRESS AS A METHOD FOR INDUCING 4D BEHAVIOUR INTO COMPOSITE LAMINATES

Christopher J. Jenkins[1], Matthew J. Donough[2] and B. Gangadhara Prusty[3]

[1]ARC Training Centre for Automated Manufacture of Advanced Composites, School of Mechanical & Manufacturing Engineering, UNSW Sydney, NSW 2052, Australia

Corresponding author (christopher.jenkins@unsw.edu.au)

Keywords: 4D printing, Prestress, Chirped fibre bragg grating sensor

ABSTRACT

Mould free manufacturing of composite structures describes the decoupling of the mould surface to part geometry. These technologies endeavour to reduce the capital tooling expenditure and add design flexibility to composite production. Recent advances in four-dimensional (4D) printing have shown the development of mouldless fibre reinforced polymer (FRP) manufacturing technologies. These could produce three-dimensional parts off a flat mould by leveraging intrinsic thermal imbalance in asymmetric laminates. This paper presents eccentric prestress, which is described as the application of pretensioned fibre offset to the neutral bending axis, as an alternate mould free methodology. The structural benefits of this approach is independent of asymmetric laminate design. Euler-Bernoulli beam theory (EBBT) and finite element (FE) methods validated the performance of laminates produced using a bespoke prestress jig. These demonstrated strong alignment between the predicted and manufactured geometry. Agreement between both embedded chirped fibre bragg grating (CFBG) sensors and external surface stain measurements to the FE model gave further confidence that the process was well described by the analytical approach. The study concluded that eccentric prestress was a viable method to produce mould free composites, critically from structurally superior, symmetric laminate configurations.

1 INTRODUCTION

Composite materials are renowned for their high specific stiffness and strength. However costs associated with manufacturing prevent broad adoption of FRP technology. This limits their application to high performance industries such as aerospace, marine, and motorsport where absolute performance outweighs component economics [1, 2]. One key driver for total manufacturing cost is the mould tooling [3]. In traditional composite manufacturing, a male or female mould surface is required to represent the inner or outer surface of a skinned laminate respectively. These mould parts are typically precision machined, and in cases of mass production, from metallic billets. The process is expensive and demands that a geometry be *"locked in"* with no changes made after the mould is commissioned. It is this expenditure and inflexibility that creates a key bottleneck in composite production.

Four-dimensional printing seeks to decouple the final geometry from the mould surface by deliberately inducing internal stress to instigate deliberate warpage of the part into a predetermined shape [4]. This is typically achieved by selective distribution of stimuli reactive material within a component such that exposure to these stimuli results in localised expansion and contraction in the component which results in a global geometric reconfiguration. These stimuli are commonly heat, light, moisture, or magnetic field however many alternates also exist [5, 6].

Historically, 4D printed structures were comprised of soft polymeric components as traditional 3D printing methods gave good control over the spatial distribution of responsive materials and so have seen application in medical devices, flexible electronics, and smart textiles [7, 8]. More recently, it has been demonstrated that 4D behaviour could be induced within FRP composites by using automated fibre placement (AFP) to perform the spatial distribution operation. Here, selective fibre orientation created internal stresses during thermal cure cycles due to the asymmetric laminate condition. This process has been used to create components such as automotive leaf springs, omega stiffeners, twisted structures, and ornamental letters of the alphabet all off a flat mould with good success [9-12].

The key restriction to this AFP style of 4D printing is the intrinsic coupling of the deformed geometry and laminate sequence. The restriction is best explained by example, as shown in the leaf spring study. To create the required asymmetry to achieve the correct radius of curvature, a $[0_{16}/90_{24}]$ laminate was employed [10]. Here 60% of the fibres were oriented transverse to the longitudinal bending stresses which characterise the only significant stress during the loaded condition of a leaf spring. This resulted in a component that was significantly heavier than required and nullified some of the key benefits FRPs offer over their metallic counterparts.

In adjacent fields, researchers have used eccentric prestress as a technique to control laminate geometry or induce bistable behaviour [13-15]. Here, select fibre was pretensioned eccentric to the neutral axis. After the curing process, this pretension was released, causing the laminate to deform as it sought equilibrium with the competing internal stresses. Critically, the studies focusing on geometric control looked at reducing warpage in asymmetric laminates and not creating a mould-geometry independence. To the knowledge of the authors, this area has been overlooked by the current body of research and could present the potential to induce 4D type behaviour, without requiring asymmetric laminate configurations.

Considering this, the paper seeks to demonstrate the feasibility of eccentric prestress to induce mould free behaviour within symmetric FRP laminates. A bespoke fibre pretension jig was developed to experimentally validate the analytical and FE models on a series of $[0_2]$, unidirectional carbon FRP laminates, with varied prestress, and give confidence that eccentric prestress was a viable process to induce deformation.

2 ANALYTICAL QUANTIFICATION OF ECCENTRIC PRESTRESS

Eccentric prestress has been represented analytically using classical laminate theory. However, EBBT presents a capable, *"low-cost"* model for determining the deformation effects in scenarios where the isotropic loading and material conditions dominate. The equilibrium equation for an unloaded eccentrically prestressed laminate is shown in Eqn. (1) and presented diagrammatically in Fig. 1 (a):

$$\sum M = -P_{fibre}e \tag{1}$$

where M is the induced moment within the laminate, P_{fibre} is the force applied to the fibre, and e is the eccentricity from the neutral axis. From EBBT, the deflection profile is then shown in Eqn. (2), where x is a variable along the beam's length such that $0 \leq x \leq l$, $v(x)$ the deflection function, and EI the flexural rigidity.

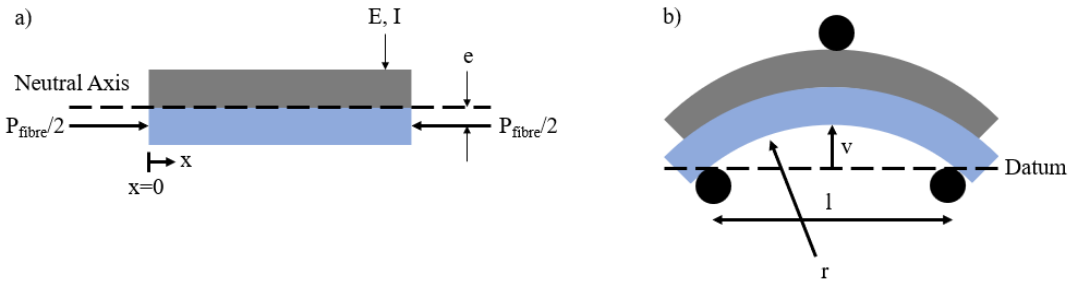

Figure 1: (a) Free body diagram of eccentric prestress side view orientation and (b) 3PB setup with deformed specimen. Prestressed fibre shown in orange and neutral fibre in grey.

$$v(x) = \frac{1}{EI}\iint_0^l \sum M \, dxdx \tag{2}$$

The stress distribution across the length of the prestressed specimen was assumed to be constant and

so the resulting profile assumed circular. To calculate the radius of curvature, the vertical deflection at the midspan of an arc with length l, being $v\left(\frac{l}{2}\right)$, gives the radius calculated in Eqn. (3). This is shown in Fig. 1 (b).

$$r = \frac{l^2}{8v\left(\frac{l}{2}\right)} + \frac{v\left(\frac{l}{2}\right)}{2} \tag{3}$$

3 MANUFACTURING METHODOLOGY

A bespoke pretension jig was designed to accommodate the model developed through EBBT. A schematic of this is shown in Fig. 2. After calibration of the jig, it was found that the combined stiffness of the spring system was 143.2 N/mm. By considering the stiffness of the fibre as $k_{fibre} = E_{11}A/l$ where the terms E_{11}, A and l refer to the modulus of the fibres, cross-sectional area, and effective length of the fibre strip respectively, Eqn. (4-6) could be used to calculate the load transferred into the fibre from the jig.

$$\{P\} = [K]\{u\} \tag{4}$$

$$\begin{Bmatrix} p_1 \\ p_2 \\ p_3 \end{Bmatrix} = \begin{bmatrix} k_{spring} & -k_{spring} & 0 \\ -k_{spring} & k_{spring} + k_{fibre} & -k_{fibre} \\ 0 & -k_{fibre} & k_{fibre} \end{bmatrix} \begin{Bmatrix} u_1 \\ u_2 \\ u_3 \end{Bmatrix} \tag{5}$$

$$P_{fibre} = E_{11}A(u_3 - u_2) \tag{6}$$

Here P represents the nodal forces, K the global stiffness matrix and u the nodal displacements. Eqn. (8) is solved by setting u_1 to the spring extension and $u_3 = 0$ whilst leaving u_2 unconstrained.

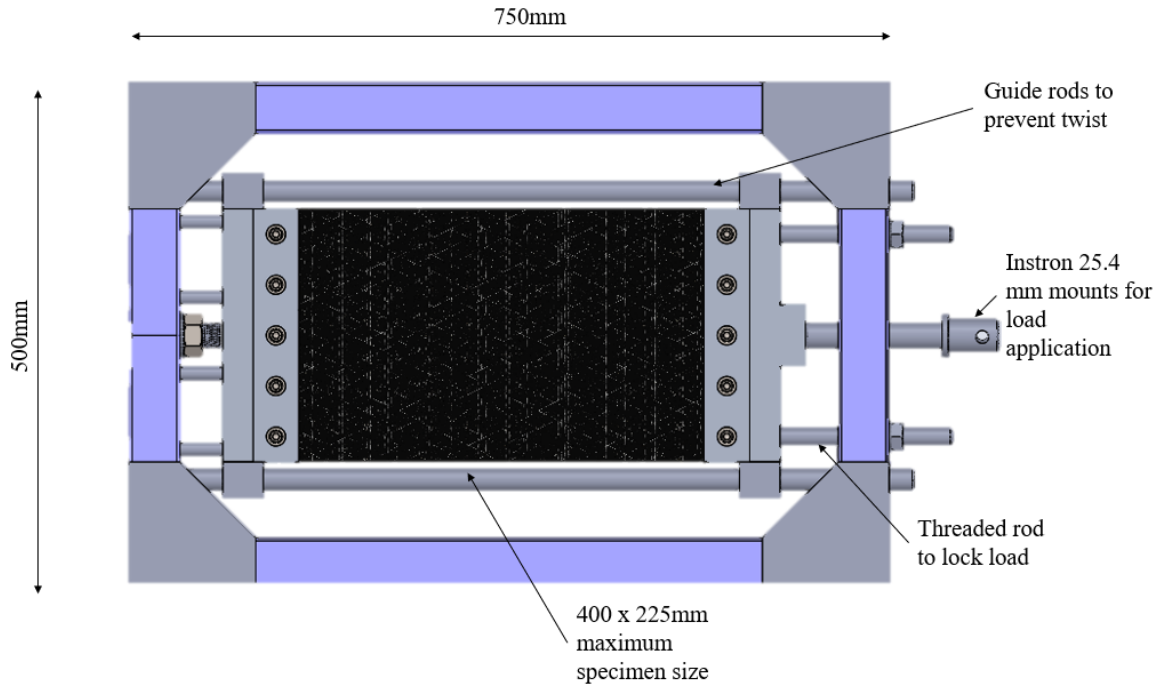

Figure 2: Schematic of the bespoke fibre pretension jig.

The specimens were produced using Toray T300 unidirectional carbon fibre and Allnex R180 epoxy resin mixed in a 5:1 ratio with H180 hardener. Traditional manufacturing methods were used under controlled laboratory conditions. The process is described in Fig. 3 and the resultant mechanical properties shown in Table 1.

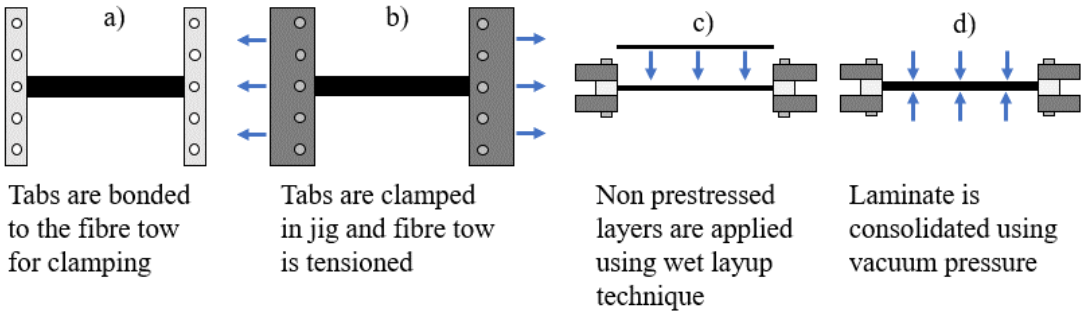

Figure 3: Specimen manufacture process: (a) tabs bonded to dry fibre tows, (b) fibre tows are prestressed in jig, (c) hand lamination with resin and (d) consolidation with top and bottom tool plates.

Laminate	Parameter	Value
Standard Modulus Carbon T300 (dry)	Elastic Modulus	230 GPa [16]
Epoxy Resin R180 (20% H180 hardener)	Elastic Modulus	2.96 GPa [17]
Carbon Epoxy (T300/R180)	Elastic Modulus	58.7 MPa

Table 1: Material properties.

Additionally, CFBG sensors were embedded within select laminates adjacent to the prestressed fibre during lamination. After cure but prior to release from the jig, surface mounted strain gauges were placed above and below the 10mm CFBG sensing element to facilitate a strain gradient measurement after release from the jig. This configuration is depicted in Fig. 4.

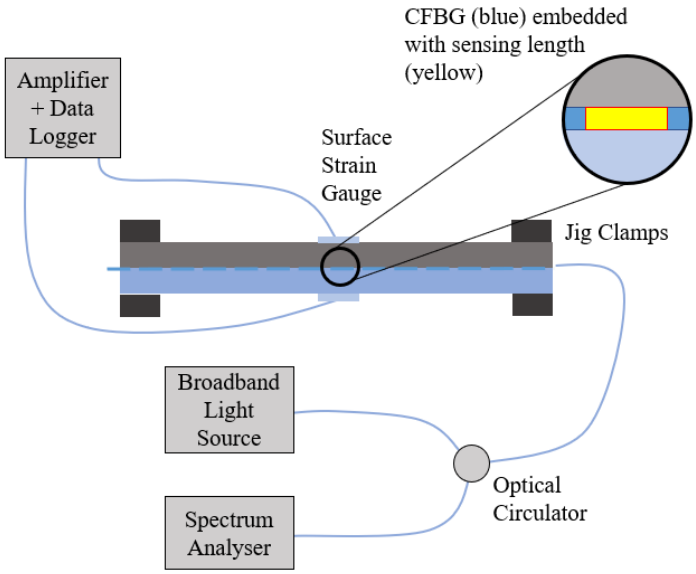

Figure 4: Experimental setup and placement of strain sensors on specimen in pretension jig.

On release from the jig, the deflection of the specimen was assessed by using a three-point bend fixture and a 3369 Instron universal testing machine. As shown in Fig. 1 (b), the vertical deflection v

measurement could be extracted by referencing the crosshead displacement at first contact with the specimen from a flat datum and subtracting the specimen thickness. A span l of 25.4 mm was used for the lower supports, facilitating the calculation of the radius using Eqn. (3).

Specimens were manufactured at 0 mm, 5 mm, 10 mm, and 15 mm of spring extension, which corresponded to approximately 0 MPa, 152 MPa, 292 MPa, and 451 MPa respectively.

4 FINITE ELEMENT QUANTIFICATION OF ECCENTRIC PRESTRESS

A non-linear, two-dimensional plane strain model was developed in ANSYS to simulate the prestress condition as defined in the manufacturing methodology. Assessment of the model's sensitivity to orthotropic properties showed that the isotropic characteristics dominated the problem, allowing the isotropic material properties presented in Table 1 to be used, only. The prestressed and neutral layers were modelled using PLANE 183 elements, achieving mesh convergence at an element size of 0.5mm.

The problem was solved using a three-step model that paralleled the manufacturing process as shown in Fig. 5.

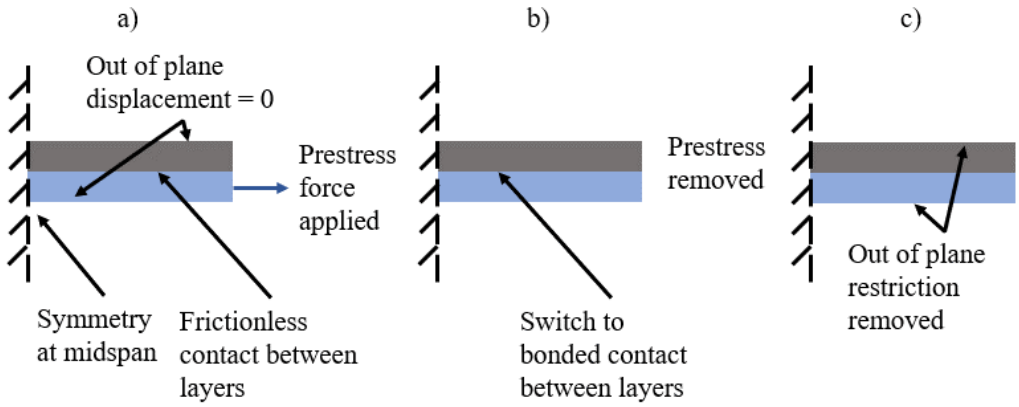

Figure 5: FE modelling steps. (a) apply load to the pretensioned layer, (b) apply bonded contact between neutral and pretensioned layer & (c) remove out of plane boundary conditions respectively.

5 RESULTS AND DICUSSION

Deflection was measured and calculated for six unique specimens and compared to FE and EBBT predicted values, shown in Fig. 6. Average prediction variation stood at 11.3% and 8.6% respectively with a reduction in standard deviation observed at increased prestress levels. This indicated that higher consistency in prestressed specimens was obtainable at high prestress and proposed to be a result of the internal stress state dominating inconsistencies within the laminate. Overall, the FE and EBBT models predict highly similar results, both recognising the non-linearity of the problem. This have confidence that the EBBT model was a suitable, *"low cost",* alternative for accurate prediction of deflection.

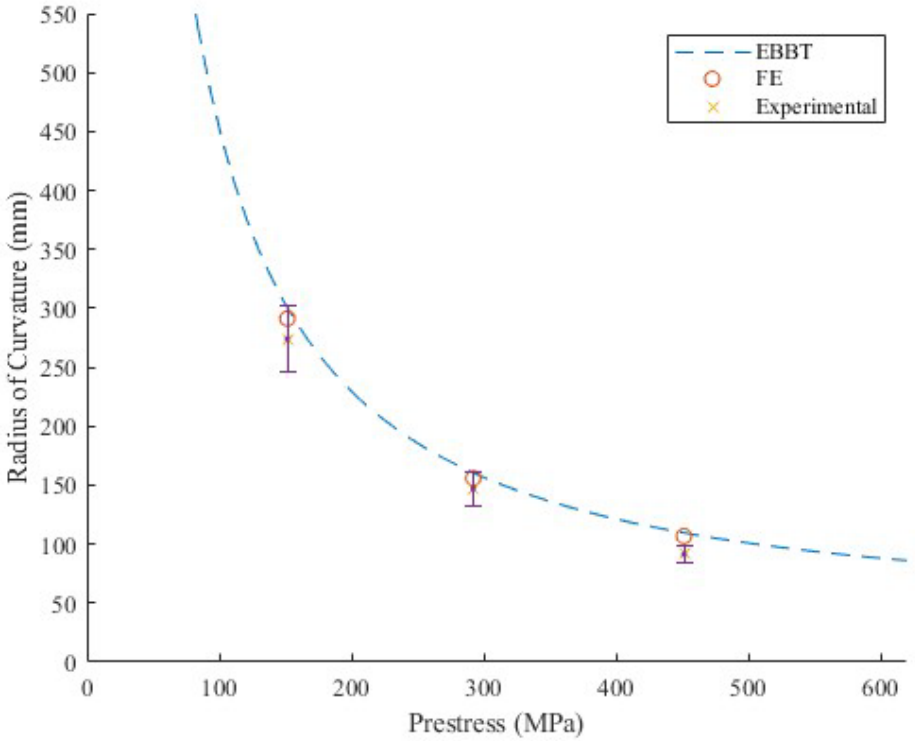

Figure 6: Experimental deflection of prestressed specimens against EBBT and FE predictions.

High circularity was observed in the specimens too, indicating the circular assumption appropriate, further reinforced by the strong alignment between the predicted and experimental deflection values. A sample of the produced specimens is shown in Fig. 7 that demonstrate this circularity.

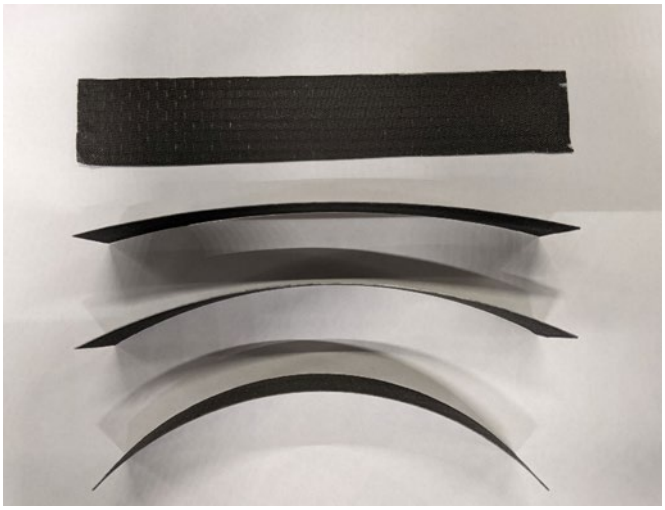

Figure 7: Prestressed specimens (lower three) and control (top).

To reinforce the accuracy of the model, the experimental strain profile was compared to the predicted FE values for both a linear and non-linear model. It was found that the linearity condition made little difference to the FE strain profile. The experimental strain is shown over time in Fig. 8.

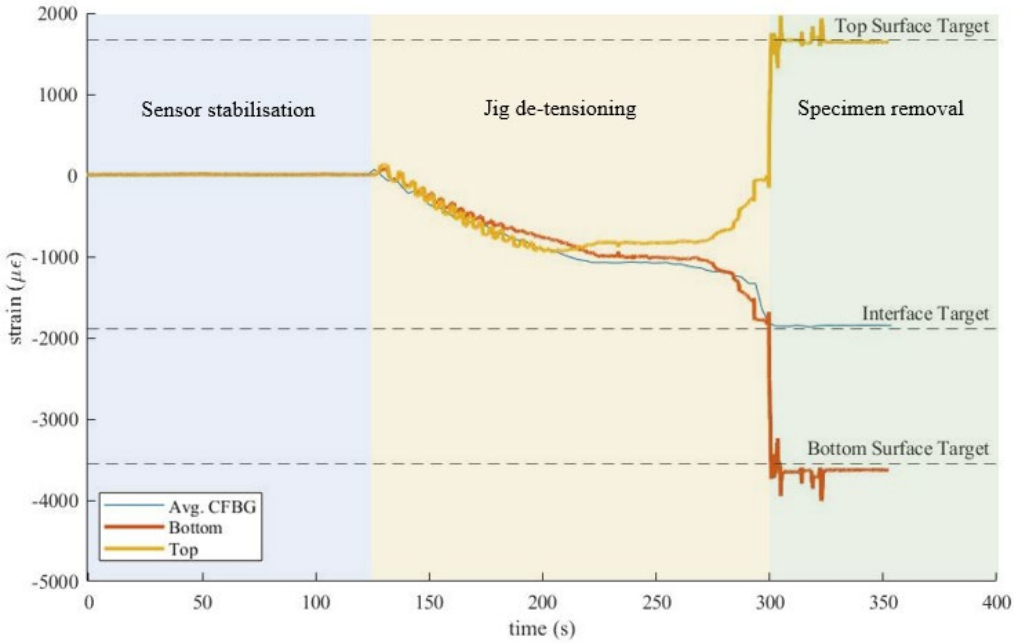

Figure 8: Experimental strain over time as specimen is removed from fixture. The 2-ply specimen was 150 × 30.7 × 0.55 mm and prestressed to 2061.3N. Referenced against FE target strain.

All three sensors showed excellent agreement to the FE surface and midplane strain targets which indicated that the model well predicted the physical experimental condition. Here the FE strain prediction was superior to EBBT, presenting a small, 3.3% average discrepancy across all three sensors whilst the EBBT method resulted in 8.6% for the same metric. The EBBT model does not consider the non-linearity of the problem, nor the subtler mechanics of the contact problem, and it is proposed that this is what drives the difference. It is recommended that an FE model be employed for strain assessment of eccentrically prestressed specimens whilst both EBBT and FE models are suitable for predicting the deflection.

9 CONCLUSIONS

The study has demonstrated that eccentric prestress can induce deformed laminates in a controlled manner from a flat mould. Importantly, these laminates were symmetric in nature and so provided a decoupled laminate-geometry methodology which rivalled AFP type 4D composites. Analytical and numerical models showed good agreement with specimens produced from the bespoke prestress jig, suggesting that eccentric prestress was a feasible method for inducing 4D type behaviour. Deflection was well predicted using both methods whilst a comparison of the internal and external strain profile, made possible by using CFBG optical sensors, showed that a FE approach was superior in extracting the final strain of a laminate. Future research in eccentric prestress will seek to assess the structural implications of the process, along with laminate optimisation by considering alternate fibre materials and combinations.

ACKNOWLEDGEMENTS

The authors would like to acknowledge the financial support received through the Australian Government Research Training Program (RTP). Furthermore, additional support came from, ARC ITTC: ARC Training Centre for Automated Manufacture of Advanced Composites (IC160100040).

REFERENCES

[1] P. T. Maung, B. G. Prusty, M. J. Donough, E. Oromiehie, A. W. Phillips, and N. A. St John, "Automated manufacture of optimised shape-adaptive composite hydrofoils with curvilinear

fibre paths for improved bend-twist performance," *Marine Structures,* vol. 87, p. 103327, 2023/01/01/ 2023, doi: https://doi.org/10.1016/j.marstruc.2022.103327.

[2] C. Zhao, M. J. Donough, B. G. Prusty, J. Xiao, L. Zhou, and L. An, "Pseudo-ductile fracture in grid stiffened structure by automated fibre placement," *Composite Structures,* vol. 308, p. 116694, 2023/03/15/ 2023, doi: https://doi.org/10.1016/j.compstruct.2023.116694.

[3] A. Ahmed, S. Arya, V. Gupta, H. Furukawa, and A. Khosla, "4D printing: Fundamentals, materials, applications and challenges," *Polymer,* vol. 228, p. 123926, 2021/07/16/ 2021, doi: https://doi.org/10.1016/j.polymer.2021.123926.

[4] Z. Ding, O. Weeger, H. J. Qi, and M. L. Dunn, "4D rods: 3D structures via programmable 1D composite rods," *Materials & Design,* vol. 137, pp. 256-265, 2018/01/05/ 2018, doi: https://doi.org/10.1016/j.matdes.2017.10.004.

[5] Q. Ji, M. Chen, X. V. Wang, L. Wang, and L. Feng, "Optimal shape morphing control of 4D printed shape memory polymer based on reinforcement learning," *Robotics and Computer-Integrated Manufacturing,* vol. 73, p. 102209, 2022/02/01/ 2022, doi: https://doi.org/10.1016/j.rcim.2021.102209.

[6] F. Momeni, S. M.Mehdi Hassani.N, X. Liu, and J. Ni, "A review of 4D printing," *Materials & Design,* vol. 122, pp. 42-79, 2017/05/15/ 2017, doi: https://doi.org/10.1016/j.matdes.2017.02.068.

[7] C. Lin, L. Liu, Y. Liu, and J. Leng, "4D printing of shape memory polybutylene succinate/polylactic acid (PBS/PLA) and its potential applications," *Composite Structures,* vol. 279, p. 114729, 2022/01/01/ 2022, doi: https://doi.org/10.1016/j.compstruct.2021.114729.

[8] S. Malekmohammadi *et al.*, "Smart and Biomimetic 3D and 4D Printed Composite Hydrogels: Opportunities for Different Biomedical Applications," *Biomedicines,* vol. 9, no. 11, 2021, doi: 10.3390/biomedicines9111537.

[9] S. V. Hoa, "Factors affecting the properties of composites made by 4D printing (moldless composites manufacturing)," *Advanced Manufacturing: Polymer & Composites Science,* vol. 3, no. 3, pp. 101-109, 2017/07/03 2017, doi: 10.1080/20550340.2017.1355519.

[10] S. V. Hoa, "Development of composite springs using 4D printing method," *Composite Structures,* vol. 210, pp. 869-876, 2019/02/15/ 2019, doi: https://doi.org/10.1016/j.compstruct.2018.12.003.

[11] S. V. Hoa and D. I. Rosca, "Formation of letters in the alphabet using 4D printing of composites," *Materials Today Communications,* vol. 25, p. 101115, 2020/12/01/ 2020, doi: https://doi.org/10.1016/j.mtcomm.2020.101115.

[12] S. Hoa, B. Reddy, and D. Rosca, "Development of omega stiffeners using 4D printing of composites," *Composite Structures,* vol. 272, p. 114264, 2021/09/15/ 2021, doi: https://doi.org/10.1016/j.compstruct.2021.114264.

[13] M. E. Tuttle, R. T. Koehler, and D. Keren, "Controlling Thermal Stresses in Composites by Means of Fiber Prestress," *Journal of Composite Materials,* vol. 30, no. 4, pp. 486-502, 1996/03/01 1996, doi: 10.1177/002199839603000404.

[14] Z. Liu, X. Zheng, W. Fan, F. Wang, S. Ahmed, and L. Yan, "An alternative method to reduce process-induced deformation of CFRP by introducing prestresses," *Chinese Journal of Aeronautics,* 2022/03/14/ 2022, doi: https://doi.org/10.1016/j.cja.2022.03.005.

[15] S. Daynes, C. G. Diaconu, K. D. Potter, and P. M. Weaver, "Bistable Prestressed Symmetric Laminates," *Journal of Composite Materials,* vol. 44, no. 9, pp. 1119-1137, 2010/05/01 2009, doi: 10.1177/0021998309351603.

[16] Toray. T300 Technical Data Sheet [Online] Available: https://www.toraycma.com/wp-content/uploads/T300-Technical-Data-Sheet-1.pdf.pdf

[17] L.-X. Gong, L. Zhao, L.-C. Tang, H.-Y. Liu, and Y.-W. Mai, "Balanced electrical, thermal and mechanical properties of epoxy composites filled with chemically reduced graphene oxide and rubber nanoparticles," *Composites Science and Technology,* vol. 121, pp. 104-114, 2015/12/16/ 2015, doi: https://doi.org/10.1016/j.compscitech.2015.10.023.